Simulation of the March 9, 1995 Substorm and Initial Comparison to Data

R. E. Lopez , C. C. Goodrich, M. Wiltberger, K. Papadopoulos

Department of Astronomy, University of Maryland, College Park, Maryland

J. G. Lyon

Department of Physics, Dartmouth College, Hannover, New Hampshire

Abstract In this study we examine a period of substorm activity that occurred on March 9, 1995. Using solar wind data as input, the event has been simulated using a 3-D MHD code. To determine how well the simulation fared, we have compared the simulation results to data. This comparison has taken two forms. The first is a comparison to individual spacecraft in the magnetotail. The second is a comparison of global energy storage and release, where we have compared the auroral heating to data-based estimates of auroral energy dissipation, as well as evaluating the variation of the open flux in the simulation. There is a generally good level of agreement between the simulation results and data. Thus our results show that MHD simulations can be used to model at least one magnetospheric substorm.

INTRODUCTION

Magnetospheric substorms represent the episodic dissipation of energy stored in the geomagnetic tail that was previously extracted from the solar wind. This energy release produces activity throughout the entire magnetosphere-ionosphere system, and it results in a wide variety of phenomena such as auroral intensifications [e.g., Akasofu, 1964], the generation of new current systems [e.g., McPherron et al., 1973], and particle acceleration up to MeV levels [e.g., Baker 1984; Lopez and Baker, 1994]. Gaining a fuller understanding substorms is an important element in characterizing the space environment, and thus is critical to the National Space Weather Initiative.

Substorms are believed to be a global magnetospheric response to the solar wind, so it seems reasonable to investigate substorms using a global simulation of the solar wind-magnetosphere interaction. Therefore we have simulated one well-observed event that occurred on March 9, 1995. The simulation code used in this study is an improved version of previously developed codes [e.g., Fedder and Lyon, 1987]. It solves the full 3-D time-dependent MHD equations over the whole magnetosphere. The simulations are not a model in the usual sense, since there are no *a priori* assumptions made about the structure of the magnetosphere. The only free parameters in the simulations are the solar wind input and the ionospheric conductivity.

To understand whether the simulation results have any relationship to reality it is important to compare those results to data. This comparison can range from a detailed comparison with individual spacecraft in the magnetosphere to more global comparisons of factors related to solar wind-magnetosphere coupling, such as estimates for energy storage and release. The ability of a simulation to reproduce individual, spatially-localized variations is a key factor to its potential use as a useful predictive tool. At the same time, even if individual observations are well-modeled, unless the global interaction is handled properly, one can have little confidence in local correspondences. In this paper we will make both kinds of comparisons for a particular well-defined isolated substorm.

Geospace Mass and Energy Flow: Results From the International Solar-Terrestrial Physics Program
Geophysical Monograph 104

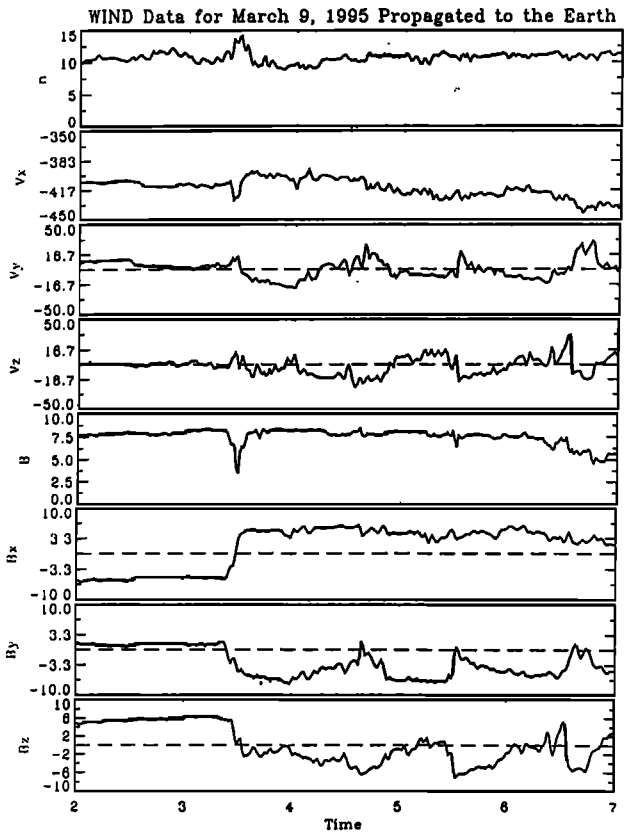

Figure 1. Wind data from March 9, 1995 shifted by 54 minutes to reflect the propagation time to Earth.

The paradigm for understanding the storage and release of energy in the magnetospheric system is centered on magnetic reconnection. When the interplanetary magnetic field is directed southward, closed flux on the dayside merges with solar wind magnetic field. This flux is transported to the tail as open polar cap flux, the polar cap grows and the flaring angle increases as the tail energy content grows [Holzer et al., 1986]. At the same time the directly-driven system dissipates some of the energy directly in the magnetosphere-ionosphere system; the input energy not dissipated is stored in the increasingly stressed configuration of the magnetotail. A global simulation that correctly includes the basic physics of solar-wind magnetosphere coupling should be able to reproduce this energy storage quite adequately.

During the substorm expansion phase, energy previously stored in the tail is rapidly unloaded. This unloading of energy must be invoked to account for the energy dissipation seen during substorms, since the output power levels can exceed the input power levels and the time history of the input and output power levels are not related by a simple time delay as one would expect in a purely driven system [Baker et al., 1986]. It is generally thought that nightside reconnection plays a key role in the dissipation of magnetotail tail flux during the substorm [e.g., Hones, 1984]. The observed variation of the open flux polar region requires reconnection [Holzer et al., 1986; Lopez 1994], though at what point in the evolution of the substorm the reconnection of lobe magnetic flux occurs is controversial [Lui, 1991; Lopez, 1994; Lopez et al., 1994; Baker 1996]. In the auroral zone the released energy is dissipated primarily through joule heating from the substorm electrojets [Akasofu, 1981]. In addition, some energy may be deposited in the ring current, while some manifests itself as plasmasheet heating.

OVERVIEW AND SIMULATION COMPARISON TO SPACECRAFT DATA

The event in question occurred on March 9, 1995, and it was identified for study by Alan Rogers of the British Antarctic Survey. Solar wind data from Wind propagated to the Earth (that is shifted by 54 minutes) are shown in Figure 1; these data were used to drive the simulation. During the last hours of March 8 and the early hours of March 9 the IMF was northward. At about 0230 UT, Wind recorded a rapid rotation of the solar wind magnetic field, including a southward turning of the IMF, that was associated with a crossing of the heliospheric plasma sheet. The southward IMF arrived at the Earth about an hour later, at 0330 UT, as seen in Figure 1. This produced a growth phase in the magnetosphere that was observed by a number of ground stations.

We have used H component data from the ground stations of the CANOPUS array using stations located near the auroral zone (63.3° to 67.3° eccentric dipole geomagnetic latitude) to construct a CL and CU, presented in Figure 2. The local field values at the start of the day as the quiet time values. Prior to substorm onset, the data do not indicate the presence of a growth phase westward electrojet. However, there was a growing (though weak)

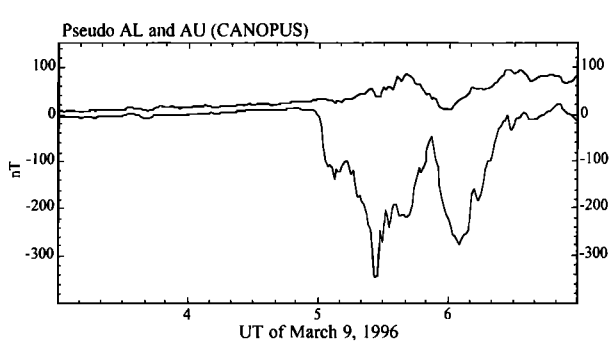

Figure 2. CANOPUS CL and CU indexes using those stations whose eccentric dipole geomagnetic latitudes range from 63.3° to 67.3°.

eastward electrojet, which is seen in the CL index as well as CU. Other ground stations (not shown) recorded a stronger growth phase signature. The data show a very clear onset at 0500 UT, an intensification at 0514 UT, some recovery, then another onset at 0552 UT, with a subsequent recovery. Through a detailed examination of CANOPUS data (along with near-by stations) we have determined that the activity was centered on the CANOPUS region. Thus these times for substorm onset and intensification are global times, even though the stations cover a limited local time sector.

Two spacecraft, Geotail and IMP 8, provide information about what happened in the magnetotail during the event. Geotail was at (-12.7, -5.2, -1.7) and IMP 8 was at (-30.3, 2.2, -9.4) in GSM coordinates. Thus Geotail was in the near-Earth dawn region, and IMP 8 was in the cislunar midnight magnetotail. Figures 3 and 4 show magnetic field and plasma data, respectively, from Geotail (dotted lines). Figure 5 shows the IMP-8 magnetic field (dotted lines). Included in all three figures are the simulations results (solid lines), which will be described in more detail below.

Figures 3 and 4 show that Geotail went through a rapid transition of the current sheet at 0458 UT, at which point

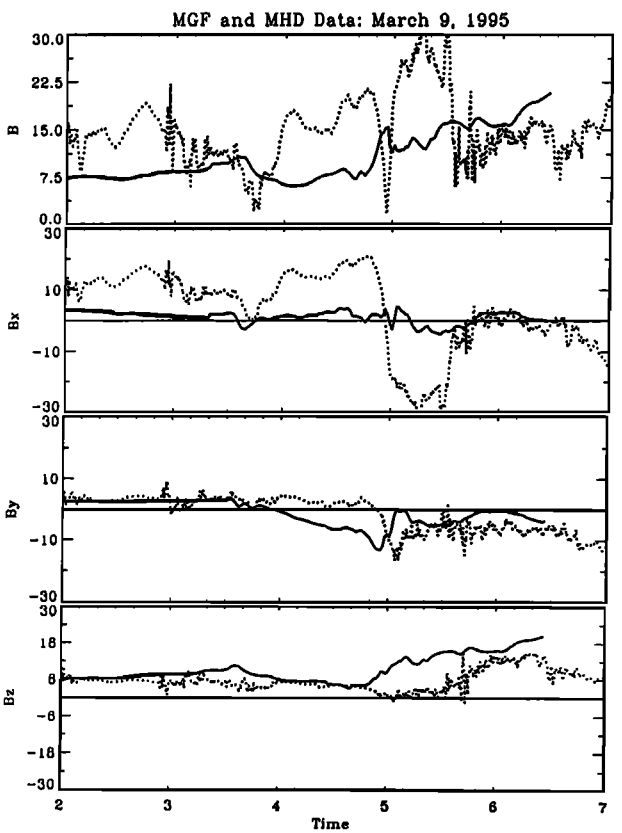

Figure 3. Geotail magnetic field data (dotted line) compared to simulation results (solid line) interpolated to the Geotail position.

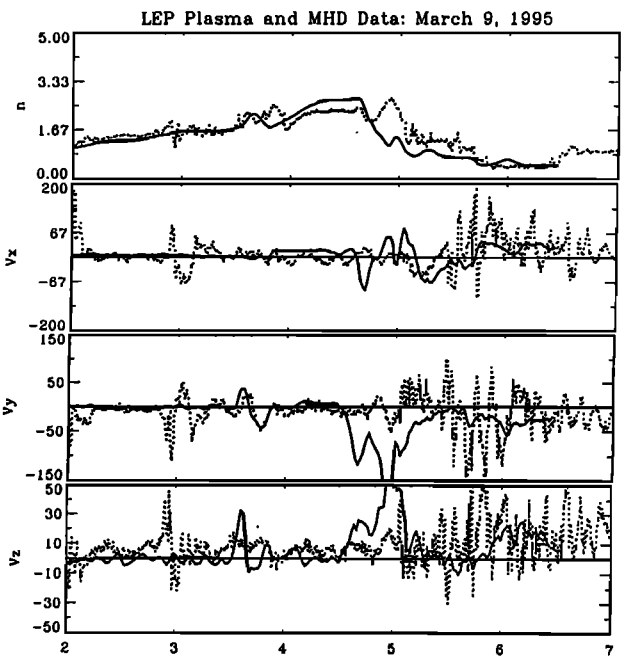

Figure 4. Geotail plasma data (dotted line) compared to simulation results (solid line) interpolated to the Geotail position.

the plasma density peaked. Just after the current sheet crossing, Geotail recorded the onset of a perturbation in the Y component that may be due to the field-aligned current in the current wedge that formed at the time with the onset of the substorm at 0500 UT. However, there was no significant dipolarization of the field, or any fast (>100 km/s) flow. This suggests that Geotail was just outside of the active sector at substorm onset. Moreover, since Geotail was on the dawn side of the active region, and in the southern hemisphere when it recorded the negative Y perturbation, the field-aligned currents producing that perturbation must have been located equatorward of the satellite - flowing on field lines that cross the neutral sheet earthward of the field lines that threaded Geotail. And since Geotail was still in the plasmasheet, the source of the substorm field-aligned currents had to be on closed field lines in the near-Earth region. Around 0525 UT, Geotail finally recorded the beginning of the local dipolarization of the field, accompanied by a number of plasma flow bursts.

Figure 5 presents magnetic field data from IMP-8, which shows a classic in the X component during the growth phase. It is interesting to note that the increase in X component began some 12 minutes after the arrival of the southward IMF on the dayside. This twelve minute delay is essentially the amount of time it would take newly merged flux to be convected to the IMP-8 location by the solar wind. At 0500 UT, a significant southward field was recorded, which is often interpreted as being due to the formation of a reconnection region earthward of the

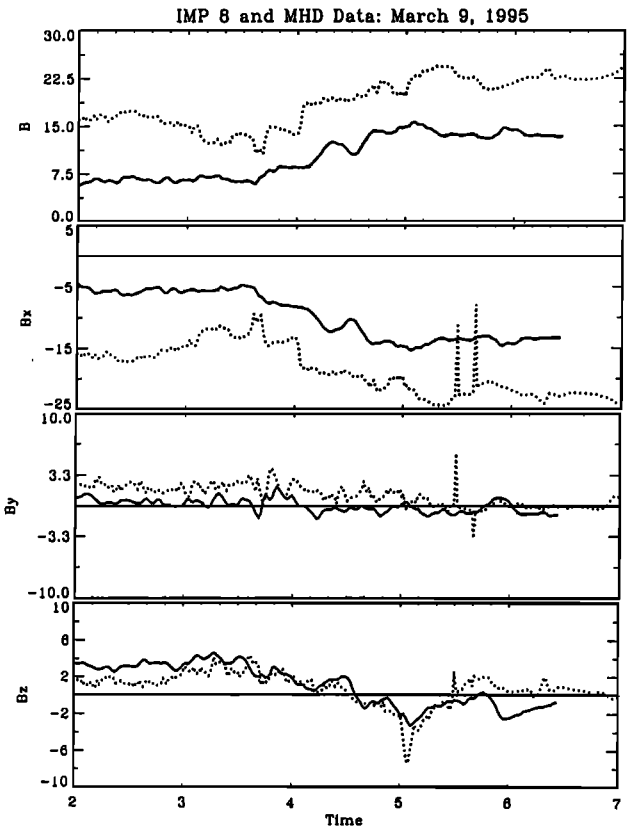

Figure 5. IMP 8 magnetic field data (dotted line) compared to simulation results (solid line) interpolated to the IMP 8 position.

satellite. However, given the proximity of IMP-8 to the lobe (as determined by the large X component), this southward field could also be due to the flaring or flapping of the tail. Interestingly enough, the filed did not weaken at this time, even though a decrease in the lobe field is often taken to signify the onset of the unloading phase of a substorm. The field did begin to weaken at 0520 UT, just after the intensification on the ground began at 0514 UT, but it began to grow again at about 0545 UT. Thus while the initial onset, or more precisely the intensification, appears to be correlated with variations at IMP-8, the 0552 UT onset does not appear to have had any significant corollary in the IMP-8 field data.

The period during which this above described substorm activity took place is well suited to simulation. There was a long period of northward IMF, which allows the simulation to relax to a "ground state", and the substorm itself was isolated and well-observed. In order to better approximate reality, such factors as dipole tilt (a constant value corresponding to 0500 UT) and the aberration due to the orbital motion of the Earth have been included. An example of the simulation result is Figure 6, which shows the density in the X-Z plane at midnight at 0455 UT. Animated sequences of the results have been produced and are available at http://www.spp.astro.umd.edu under "Global simulations". To compare the simulation with the spacecraft data, we have interpolated the simulation results to the spacecraft positions as a function of time. The simulation data are plotted as solid lines in Figures 3, 4, and 5.

The X component in Figure 3 shows apparently little agreement between data and simulation until after 0530 UT, however this initial impression is somewhat misleading. If we inspect the current sheet crossing just before 0500 UT, we see that the rapid nature of the crossing from essentially north lobe to south lobe suggest that Geotail encountered a thin current sheet a fraction of an Earth radius in north-south extent. That kind of a current sheet cannot be modeled by the simulation, whose spatial grid in the relevant region is coarser that the actual current sheet thickness. Therefore it is no surprise that the simulated magnetic field does not produce the extreme variations seen in the data, since in the simulation Geotail is embedded in a much broader current sheet.. However, we note that roughly at the time of the real current sheet crossing, the simulated current sheet center also moved past the Geotail position, so that in the simulation Geotail moved from the northern hemisphere to the southern hemisphere at about the right time. In the light of this consideration, the discrepancies seen the upper panel (field magnitude) become more reasonable.

The simulated Y and Z components show a much better agreement with the data, though there is an important exception. The local onset of the substorm (as marked by dipolarization) is a bit early in the simulation when compared to the data. The Y component shows a deflection that we associate with the field-aligned current in the substorm current wedge. That deflection starts a bit earlier in the simulation than in the data, though the magnitude and shape of the deflection are very similar. The rise in the Z component we associate with the dipolarization due to the substorm current wedge. Again this begins earlier in the simulation that in reality. In fact, Geotail did not see a the onset of the dipolarization until about 0525 UT, which we associate with the substorm intensification at 0515 UT.

Both the simulation results and the data are consistent with the formation of a current wedge just to the west of Geotail (in accord with the ground data) that spread eastward as the substorm intensified. It is just that the simulated current wedge formed a bit early and arrived at Geotail a bit early. Some of this timing discrepancy could be due to a spatial resolution effect, since in reality the current wedge was more spatially confined than in the simulation. Nonetheless, after the substorm has subsided by 0600 UT, there is remarkably good agreement between the simulation and all three components of the magnetic field. It is at this time that one would expect that the current sheets were no longer thin, supporting our interpretation that the

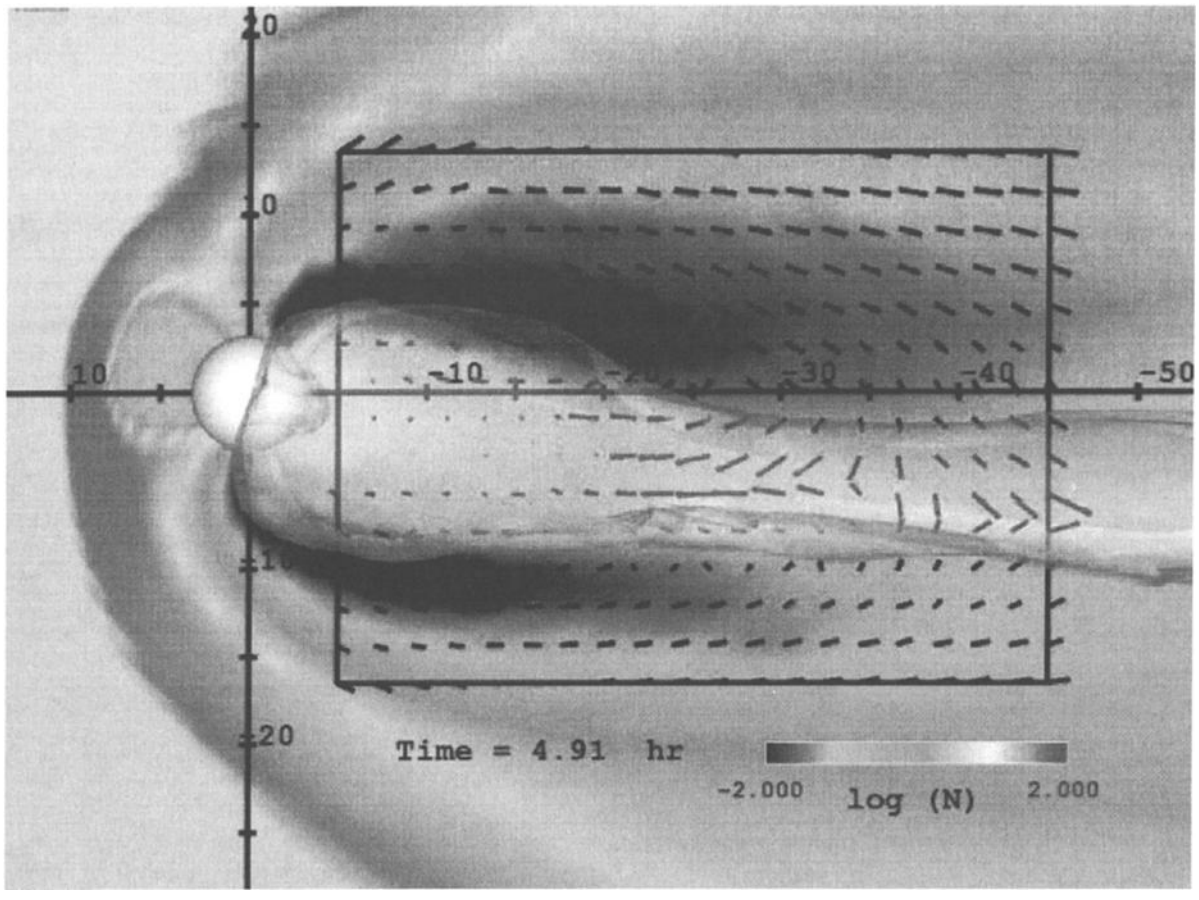

Figure 6. A sample of the simulation results. The figure shows the plasma density in the X-Z plane in the midnight meridian at 0455 UT. The arrows within the box show the flow field. The white circle denotes the inner edge of the simulation at about 3 Earth radii. The open-closed field line boundary is shown as a transluscent surface.

agreement is really rather good in a qualitative sense, and that the source of quantitative discrepancy between the Geotail field observations and the simulation has to do with issues of spatial resolution and the inability of the current code to reproduce the thin current sheets observed in nature.

The Geotail plasma data, along with the simulation results, are presented in Figure 4, and again the simulation is the solid line. The overall agreement is good, especially for the density. The high-speed, short duration flow events are not well-represented by the simulation, but again given spatial resolution issues one would not expect to see them. The biggest discrepancy concerns the onset of the activity at and before 0500 UT. The simulation predicts large Y and Z velocities that were not seen, although velocities of similar magnitude, if not duration, were observed a bit later. This discrepancy is probably related to the current wedge issues discussed above, since the curl of the velocity field drives field-aligned currents.

Figure 5 shows the IMP 8 magnetic field and the simulation results (solid line). The agreement with the Z component is remarkable, and the Y component is also very good. The simulated X component, however, is always of lesser magnitude than the data, which in turn drives the total field magnitude to be lower than observed. Part of this discrepancy may be due to the same issue of spatial resolution discussed above that produces a thicker current sheet, and hence a smaller X component at the IMP 8 position. However, this is not the entire story. The maximum lobe field strength in the simulation at the IMP 8 distance down the tail just before the onset is only about 18 nT, which is still lower that the observed lobe field of 25 nT at the same time. This suggests that the flaring of the magnetosphere in the simulation was less than in reality, which in turn suggests that the amount of flux transported into the lobes was less in the simulation than actually occurred. In fact, we have a possible resolution to this discrepancy (discussed in the next section), namely that

extra energy was dissipated in the ionosphere and so this energy did not appear as tail lobe flux.

Despite the discrepancies, we feel that the simulation has done a very credible job in reproducing point measurements in the magnetosphere. We also feel that we understand the major contributions to these discrepancies, and that improvements in the code will lessen their impact. We now turn to a comparison between the global evolution of the code and what can be determined from data, using the evolution of the total energy budget as the organizing principle for that comparison.

ENERGY INPUT AND DISSIPATION: OBSERVATIONS

We may estimate the energy input into the magnetosphere during the event by using the epsilon parameter [Akasofu, 1981], shown in Figure 7. The solar wind data and resulting energy input have been lagged by 54 minutes to reflect the propagation time to Earth, and a merging line length of 7 Re was assumed. By 0630 UT, we estimate that 760 gigawatt-hours had been provided to the magnetosphere by the solar wind.

Estimates of the power dissipated in the auroral zone by electrojet joule heating have used AE as the indicator of electrojet strength [Akasofu, 1981; Baumjohann and Kamide, 1984]. Because our observations are from a limited local time sector, and thus do not reflect the entire auroral zone, our CANOPUS-derived AE index is very likely an underestimate of electrojet activity, since the maximum in the eastward or westward electrojet may be outside of the CANOPUS array. However, we may use the CANOPUS data to estimate the heating at a given time, provided that we can safely presume that the CANOPUS station do in fact lie in the region of maximum eastward or westward electrojet. During the substorm onset and expansion we are very confidant that this was very likely the case with regard to the westward electrojet, and we will use CANOPUS CL to calculate the dissipated energy. During the growth phase this does not seem to be the case with regard to either the eastward or westward electrojets. However, the response of the stations was more due to the eastward, rather than to the westward, electrojet, and so for the growth phase we will use CANOPUS CU. After 0630 UT, the CE we can derive from CANOPUS seems adequate.

Baumjohann and Kamide [1984] found that the joule heating (in gigawatts) produced by the eastward and westward electrojets is 0.42 AU and 0.25 AL, respectively, while the overall joule heating is 0.32 AE. Using these results we can estimate that the joule heating from both eastward and westward electrojets is approximately 0.54 AL. Thus from 0500 UT until 0630 UT, we estimate that 127 gigawatt-hours were dissipated as joule heating in the northern hemisphere. In the growth phase the CANOPUS

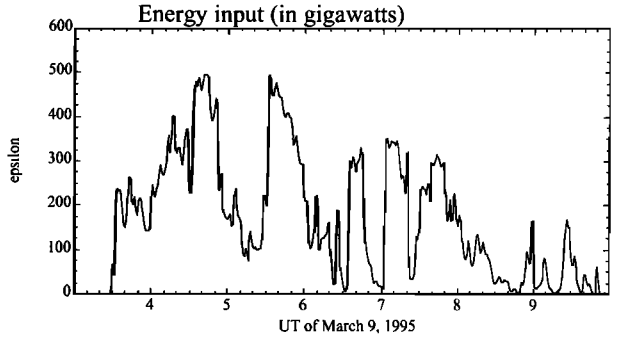

Figure 7. Solar wind energy input (epsilon) for March 9, 1995 lagged by 54 minutes to reflect the propagation time to Earth.

chain was responding primarily to the eastward electrojet. We now use Baumjohann and Kamide [1984] to estimate that the total heating from both eastward and westward electrojets is approximately 0.77 AU. This yields an energy dissipation in the northern auroral zone from 0330 UT to 0500 UT of 28 gigawatt-hours (prior to 0330 UT there was essentially no dissipation). Thus the total joule dissipation in the northern hemisphere from 0300 UT to 0630 UT can be estimated at 155 gigawatt-hours, which we in fact regard as a lower limit.

To get an estimate for the total dissipation, north and south, we could simply double the northern estimate, yielding a total dissipation of 310 gigawatt-hours. However, during the event there was a significant dipole tilt, making the southern hemisphere the sunlit hemisphere. Because of the enhanced conductivity, the simulation produces southern auroral zone currents that are bigger that the northern ones, and the energy dissipation in the southern ionosphere is almost twice as large as that in the northern ionosphere. We have no southern hemisphere data which we can directly compare to the CANOPUS data, however, if this current asymmetry was indeed the case, then the total auroral zone dissipation from 0330 UT to 0630 UT was roughly 465 gigawatt-hours.

Another major sink for energy is ring current injection. Using the pressure-corrected Dst values [Akasofu, 1981; Zwickl et al., 1987], the power dissipated may be estimated by

$$K\left(\frac{Dst^{pc}}{\tau} + \frac{\partial Dst^{pc}}{\partial t}\right)$$

where $K=4\times10^{13}$ joules/nT, and τ is the ring current decay time, which we take to be six hours. We have obtained the provisional hourly Dst from the WDC-C2 for Geomagnetism, Kyoto University, web site (from 0000 UT to 0800 UT, hourly Dst values were 3, 4, 8, 8, 5, 1, -3, -4). Using the above equation we find that the energy dissipated into the ring current from 0330 UT to 0630 UT was roughly 130 gigawatt-hours. Thus in our event the auroral dissipation was the largest sink for magnetospheric energy.

Combining the energy input to the ring current with the dissipation of energy in the auroral zone energy suggests that from 0330 UT to 0630 UT, roughly between 440 and 595 gigawatt-hours were dissipated in the magnetosphere, depending on whether you take the lower or higher estimate for the auroral dissipation. Our estimate of the energy input during the same time period is 760 gigawatt-hours. Thus between 58% and 78% of the input energy appears to have been dissipated. It might be tempting to assume that the remaining energy was expelled as a plasmoid. However, subsequent activity in the magnetosphere ran a significant energy deficit. From about 0715 UT to 0915 UT there was a period of much stronger activity that in the northern ionosphere alone dissipated 280 gigawatt-hours (using our proxy AL and the same assumptions as the above calculation). In the same period the estimate for energy input using epsilon in 230 gigawatt-hours. Thus it is unlikely that the initial activity used up all of the input energy, since some storage until the subsequent period of activity is needed to account for the energy budget from 0715 UT to 0915 UT. Given these considerations, there does not seem to be to much room for a plasmoid to contribute significantly to the energetics of this event.

ENERGY CONSIDERATIONS: COMPARISON WITH THE SIMULATION

Figure 8 presents the simulated polar cap flux (where the polar cap is defined as the open-closed field line boundary and the flux is integrated over both hemispheres), and Figure 9 shows the polar cap boundaries along the noon and midnight meridians. At 0335 UT the polar cap began to grow. The growth was initially on the dayside, a direct response to dayside merging. The midnight boundary did not move substantially equatorward until about 25 minutes later. If we consider that newly merged field lines are anchored at one end in the solar wind (which was flowing at about 400 km/s), a 25 minute time delay suggests that the field line have been convected about 100 Re downstream (roughly the nominal tail length) before the

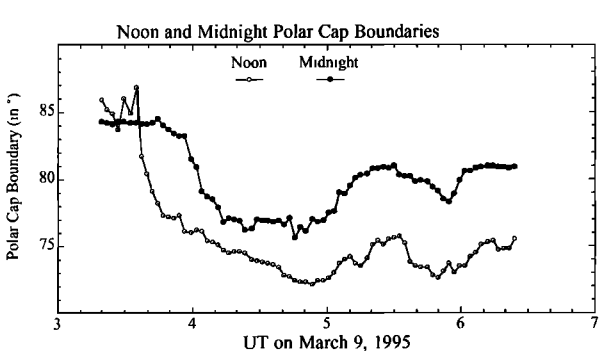

Figure 8. Simulated polar cap flux (total, both hemispheres).

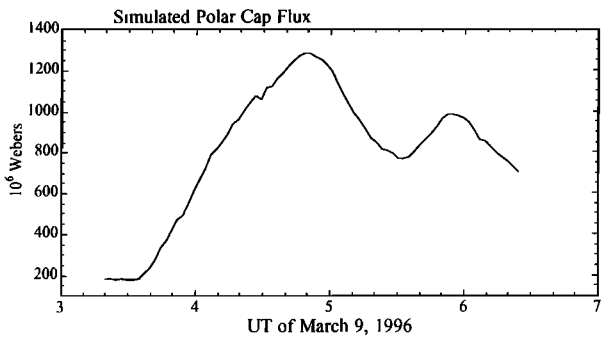

Figure 9. The noon and midnight latitudes of the northern open-closed field line boundary.

growth of the polar cap hits midnight. The polar cap continued to add flux until about 0454 UT, when the polar cap began to shrink, although reconnection of lobe field lines (and thus onset) began a couple of minutes earlier. The rate of flux decrease increased dramatically at 0503 UT and continued until about 0530 UT, when the polar cap began to grow again. At 0556 UT the polar cap began to shrink once more.

Each of these episodes of polar cap shrinkage correspond to the unloading of stored energy as represented by magnetic flux. Comparing to the data in Figure 2 we see that in fact the initial onset (0500 UT in the data, 0452 UT in the simulation) the intensification (0514 UT in the data, 0503 UT in the simulation), and the second onset (0553 UT in the data, 0556 UT in the simulation) were all captured by the simulation, though the temporal correspondence is not perfect. Another issue is that the slight decrease in polar cap flux at 0440 UT (which we call a pseudobreakup) did not correspond to any real activity. On the other hand, it is clear that at 0630 UT, not all of the stored energy has been released, as was surmised from the data-based estimate above. This is consistent with the suggestion that stored energy must be carried over to the later period of activity in order to account for the inferred energy budget. It is also consistent with the fact that the simulation did not develop much of a plasmoid. Thus in terms of both qualitative and quantitative behavior of the polar cap flux, our simulation is substantially in accord with the observations.

We have also carried out calculations of the joule heating for both auroral zones, and these are presented in Figure 10. There are areas of agreement, and of discrepancy, when we compare to the dissipation estimates made from the data. One general feature is that both the simulation and the data point to two episodes of significant heating corresponding to the two major onsets. Both show that the first period of activity was of longer duration that the first, and the average level of power dissipation was slightly greater during the second period (the data averages are 90 gigawatts versus 93 gigawatts). However, substorm

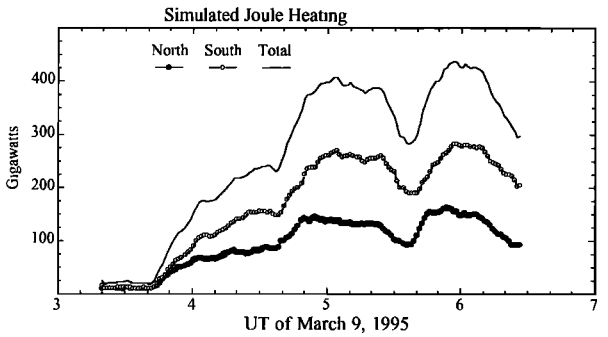

Figure 10. Simulated joule heating for northern and southern hemispheres, along with the total dissipation.

onset in the simulation began several minutes before substorm onset in the data. As pointed out above, in the simulation lobe reconnection began before the onset at 0500, and plasmasheet reconnection began even earlier. Reconnection in the simulation is driven numerically, and therefore is to some degree dependent upon the scale-size of the cells used in the computation. As the spatial resolution is increased, the development of reconnection regions can be slowed. Thus we expect that the exact time at which lobe reconnection would occur in a higher-resolution runs (which we plan to do) would likely be delayed.

Another issue regards the exact power levels. The simulation indicates that from 0330 UT to 0630 UT, 839 gigawatt-hours were dissipated, about twice as much as the data suggest. However, a close inspection of the simulation suggests that there is an effect (which we also believe to be related to spatial resolution issues) that produces an eastward electrojet that is much too large. Prior to the onset the dissipation power of around 225 gigawatts was driven primarily by this large eastward electrojet. An interesting point to consider is that if the simulation is artificially dissipating too much energy in the ionosphere then there must be correspondingly less energy stored in the lobes. This might be related to the discrepancy noted above between the observed IMP 8 magnetic field magnitude and the simulated lobe field at the IMP 8 position. If extra energy is dissipated in the ionosphere, there will be less flux in the lobes, resulting in a smaller flaring angle, and thus changing the pressure balance conditions that determine the lobe field magnitude, producing a weaker lobe field.

As an ad hoc correction we subtract 175 gigawatts from the level of ionospheric dissipation after the onset, and hold the dissipation level during the growth phase to be 50 gigawatts (similar to that observed) to estimate the actual power dissipated. The energy dissipated from 0330 UT to 0630 UT now becomes 382 gigawatt-hours, which is very close to the number derived from the data. With this correction we see that the agreement with the CANOPUS data is quite reasonable. For example, the energy dissipated in the northern hemisphere according to CL from 0500 UT to 0552 UT was 78 gigawatt-hours, yielding a total dissipation in both hemisphere of between 156 and 234 gigawatt-hours, whereas the corrected simulated northern dissipated energy was 71 gigawatt-hours and the energy dissipated in both hemispheres was 196 gigawatt-hours. Similar agreement is found for other periods, and by 0630 UT the observed northern auroral power dissipation (using CANOPUS CL) was about 35 gigawatts, which compares well with a corrected northern auroral simulated power dissipation at 0630 UT of 33 gigawatts. However, at no point does the simulation produce a peak corrected northern hemisphere power dissipation of 184 gigawatts, as was observed at 0526 UT.

CONCLUSIONS

In this paper we have presented a comparison of both single point measurements of plasma and magnetic field as well as global estimates of energy storage and release to outputs of a simulation driven with actual solar wind data. There is remarkable degree of correspondence between the observations and the simulation. The single-point measurements show qualitative, and sometimes quantitative agreement with the simulation.. Both the data and the simulation show the two substorm onsets, and the energy budgets are consistent with each other once one makes allowances for the unphysical eastward electrojet that develops in the simulation.. There are also areas of disagreement, such as the exact values of the various quantities compared at the spacecraft locations, the exact levels of auroral dissipation in the simulation versus the observations (especially the spurious eastward electrojet), and the exact times for substorm onset and intensification, that need to be addressed. We have some indications that increasing the spatial resolution in the code will help with many of these issues. Nonetheless, the results are very encouraging, since the ability to simulate the global flow of energy in the magnetosphere-ionosphere system as well as the environment in specific regions of space is a crucial step in creating a viable space weather system

Acknowledgments. The authors would like to thank T. Mukai and S. Kokubun for Geotail plasma and magnetic field data, respectively, R. Lepping for the Wind and IMP 8 magnetic field data, A. J. Lazarus for the Wind plasma data, and J. C. Samson for providing the CANOPUS data and for stimulating discussions and comments. We also wish to thank WDC-C2 for Geomagnetism, Kyoto University, for providing provisional Dst on-line. This work was supported by NASA grants NAG-56256, NAG-54662, and NAGW-3222, and by NSF grant ATM-9527055.

REFERENCES

Akasofu, S.-I., The development of the auroral Substorm, *Planet. Space Sci., 12*, 273-282, 1964.

Akasofu, S.-I., Energy coupling between the solar wind and the magnetosphere, *Space Sci. Rev., 28,* 121, 1981.

Baker, D. N., Particle and field signatures of substorms in the near magnetotail, in *Magnetic Reconnection in Space and Laboratory Plasmas*, edited by E. W. Hones, Jr., 193-202, AGU, Washington, D. C., 1984.

Baker, D. N., T. A. Fritz, R. L. McPherron, D. H. Fairfield, Y. Kamide, and W. Baumjohann, Magnetotail energy storage and release during the CDAW 6 substorm analysis intervals, *J. Geophys. Res., 90,* 1205-1216, 1986.

Baumjohann, W., and Y. Kamide, Hemispherical joule heating and the AE indices, *J. Geophys. Res., 89*, 383, 1984.

Fedder, J. A. and J. G. Lyon, The solar wind-magnetosphere-ionosphere current-voltage relationship, *Geophys. Res.. Lett., 14*, 880-883, 1987.

Holzer, R. E., R. L. McPherron, and D. H. Hardy, A quantitative empirical model of the magnetospheric flux transfer process, *J. Geophys. Res., 91,* 3287-3293, 1986.

Hones, E. W., Jr., Plasma sheet behavior during substorms, in *Magnetic Reconnection in Space and Laboratory Plasmas*, edited by E. W. Hones, Jr., 178-184, AGU, Washington, D. C., 1984.

Lopez, R. E., On the role of reconnection during substorms, *Proc. International Conference on Substorms-2*, 175-182, 1994

Lopez, R. E., C. C. Goodrich, G. D. Reeves, R. D. Belian, and A. Taktakishvili, Mid-tail plasma flows and the relationship to near-Earth substorm activity: A case study, *J. Geophys. Res., 99*, 23561-23569, 1994.

Lopez, R. E., and D. N. Baker, Evidence for particle acceleration during magnetospheric substorms, *Ap. J. S., 90*, no. 2, 531-539, 1994.

Lui, A. T. Y., A synthesis of magnetospheric substorm models, *J. Geophys. Res., 96*, 1849, 1991.

McPherron, R. L., C. T. Russell, and M. P. Aubry, Satellite studies of magnetospheric substorms on August 15, 1968: 9. Phenomenological model for substorms, *J. Geophys. Res., 78,* 3131-3149, 1973.

Siscoe, G. E. Hilner. T. L. Killeen, L. J. Lanzerotti, and W. Lotko, Developing Service Promises Accurate Space Weather Forecasts in the Future, *EOS, 75*, no 31, 365-366, August 2, 1994.

Zwickl, R. D., L. F. Bargatze, D. N. Baker, C. R. Clauer, and R. L. McPherron, An evaluation of the total magnetospheric energy output parameter, Ut, in *Magnetotail Physics*, edited by A. T. Y. Lui, 155-159, Johns Hopkins University Press, 1987.

C. C. Goodrich, R. Lopez, and K. Papadopoulos, all at Department of Astronomy, University of Maryland, College Park, MD, 20742

J. G. Lyon at Department of Physics, Dartmouth College, Hannover, NH, 03755

M. Wiltberger, Department of Physics, University of Maryland, College Park, MD, 20742